

RESEARCH

Open Access



# Last but not least: high-temperature behavior of drugmanite and comparative crystal chemistry of the gadolinite supergroup minerals under extreme conditions

Liudmila A. Gorelova<sup>1\*</sup>, Anastasiia K. Shagova<sup>1</sup>, Oleg S. Vereshchagin<sup>1\*</sup>, Dmitrii V. Pankin<sup>1</sup>, Natalia S. Vlasenko<sup>1</sup>, Iliia V. Korniaikov<sup>1</sup> and Anatoly V. Kasatkin<sup>2</sup>

\*Correspondence:

Liudmila A. Gorelova  
l.gorelova@spbu.ru  
Oleg S. Vereshchagin  
o.vereshchagin@spbu.ru  
<sup>1</sup>St. Petersburg State University,  
University Emb. 7/9, St. Petersburg,  
Russia 199034  
<sup>2</sup>Fersman Mineralogical Museum,  
Russian Academy of Sciences,  
Moscow, Russia

## Abstract

Gadolinite supergroup minerals (GSM) are common in nature and widely known as important rare earth elements (*REE*) carriers, which makes them prominent objects for study both in geology and material science. Their behavior under extreme conditions (high pressure and/or high temperature) could shed light on geochemical cycles of rare lithophile elements (e.g., *REE*, B, Be) and show the ways of transformation of crystal structures in a series of solid solutions. In this paper, we present new data on drugmanite,  $Pb_2Fe^{3+}(PO_4)(PO_3(OH))(OH)_2$ , and compare the obtained results with other GSM. Drugmanite is the least stable member of the supergroup under high temperature conditions, which is a result of the low density of the octahedral layer in its crystal structure. The beryllium silicate members of GSM were found to be the most stable in high-temperature conditions, whereas beryllium phosphate members are most stable at high pressures. The mechanisms of mineral deformation under extreme conditions are primarily determined by the composition of the tetrahedral layer and then by the size and charge of the large cations.

**Keywords** Drugmanite, Gadolinite supergroup, High temperature, High pressure, Review

## 1 Introduction

Gadolinite supergroup minerals (GSM) have been known since the 18th century (e.g [1–3]), can form fairly large crystals (up to several cm) and are the primary source of most of the rare earth elements (*REE*) [4]. GSM can be found in granitic pegmatites, volcanic and metamorphic rocks, and skarns [5–8]. They are also important geochemical markers used in provenance studies [9–11], whereas their synthetic analogues are of interest due to their unique physical and chemical properties [12–16].

Gadolinite supergroup contains 13 valid mineral species with the general formula  $A_2MQ_2T_2O_8\phi_2$ , where *A* – Ca, Pb, *REE*, *M* –  $Fe^{2+}$ ,  $Fe^{3+}$  or vacancy ( $\square$ ), *Q* – B, Be or



© The Author(s) 2025. **Open Access** This article is licensed under a Creative Commons Attribution-NonCommercial-NoDerivatives 4.0 International License, which permits any non-commercial use, sharing, distribution and reproduction in any medium or format, as long as you give appropriate credit to the original author(s) and the source, provide a link to the Creative Commons licence, and indicate if you modified the licensed material. You do not have permission under this licence to share adapted material derived from this article or parts of it. The images or other third party material in this article are included in the article's Creative Commons licence, unless indicated otherwise in a credit line to the material. If material is not included in the article's Creative Commons licence and your intended use is not permitted by statutory regulation or exceeds the permitted use, you will need to obtain permission directly from the copyright holder. To view a copy of this licence, visit <http://creativecommons.org/licenses/by-nc-nd/4.0/>.

vacancy ( $\square$ ),  $T$  – Si, As, P,  $\phi$  – O, F or OH [17]. It is divided into two groups depending on the chemical composition of the  $T$  tetrahedral site: gadolinite group (silicates) and herderite group (phosphates and arsenates). The division into subgroups is according to the chemical composition of the  $Q$  tetrahedral site (gadolinite (beryllosilicates), datolite (borosilicates), herderite (beryllophosphates and beryllarsenates) and drugmanite (phosphate)).

High temperature / high pressure behavior of datolite, gadolinite and herderite subgroup of GSM has been studied [18–25], while no data on drugmanite subgroup are available so far. Like other GSM, drugmanite ( $\text{Pb}_2\text{Fe}^{3+}\square_2(\text{PO}_4)(\text{PO}_3(\text{OH}))(\text{OH})_2$  or  $\text{Pb}_2\text{Fe}^{3+}\square_2(\text{P}_2\text{O}_7)(\text{OH})(\text{OH})_2$ ) has monoclinic ( $P2_1/c$ ) crystal structure, which can be described as consisting of two different alternating layers, one of which is formed by  $\text{TO}_4$  and  $\text{QO}_4$  tetrahedra, and another one by  $\text{AO}_6\phi_2$  polyhedra and  $\text{MO}_4\phi_2$  octahedra [17]. However, in the drugmanite crystal structure, the  $Q$  site is vacant [26], i.e. the tetrahedral 'layer' consists of isolated  $\text{PO}_4$  tetrahedra, which should lead to distinct thermal behavior.

The aim of this work is to obtain and analyze data on the high-temperature behavior of drugmanite. Including this new data, the information on high-temperature and high-pressure behavior of the GSM has been summarized. We have also analyzed the stability ranges and transformation pathways of GSM depending on chemical composition and have discussed possible implications for the prediction of thermal behavior of other isostructural minerals.

## 2 Materials and methods

The studied sample of drugmanite originates from its type locality – Richelle, Wallonia, Belgium. The plate-like crystal under study was  $0.1 \times 0.03 \times 0.02$  mm and colorless. This mineral was studied by scanning electron microscopy (SEM), energy-dispersive X-ray spectroscopy (EDS), Raman spectroscopy (ambient conditions) and single-crystal X-ray diffraction (SCXRD) under ambient and high-temperature (HT) conditions.

The chemical analyses (5 spots) were carried out using a Hitachi S-3400 N (Hitachi, Japan) SEM equipped with an EDS Oxford X-Max 20 detector (Oxford, UK). Analytical conditions were 20 kV accelerating voltage, 2 nA beam current, and a beam diameter of 1  $\mu\text{m}$ . The amount of  $\text{H}_2\text{O}$  was calculated by stoichiometry based on 10 oxygen atoms per formula unit (apfu).

The thermal behavior of drugmanite was studied in situ upon heating in air by SCXRD analysis, which was performed using a XtaLAB Synergy-S (Rigaku Oxford Diffraction, Japan) diffractometer equipped with a HyPix-6000HE detector with monochromated  $\text{MoK}\alpha$  radiation ( $\lambda[\text{MoK}\alpha] = 0.71073 \text{ \AA}$ ) at 50 kV and 1 mA with a high-temperature FMB system (Oxford, UK). More than a hemisphere of three-dimensional data was collected with a frame width of 0.30–0.75°, depending on temperature. The ambient temperature experiment was performed using a single crystal, mounted on a quartz glass fiber, whereas for the high-temperature experiments, the same crystal was placed inside a quartz capillary (for more details, see [27, 28]). SCXRD data was collected in two steps: at room temperature and upon heating (HT) at different temperatures in the range of 100–400 °C with temperature steps of 100 °C. Temperature determination errors were  $\pm 10$  °C (see [22]). The data were integrated and corrected for background, Lorentz, and polarization effects. An empirical absorption correction based on spherical harmonics

implemented in the SCALE3 ABSPACK algorithm was applied in the CrysAlisPro program [29].

The structure model of drugmanite [26] was used as a starting model for the structure refinement at all temperature points (Table S1). The positions of H atoms are undetermined. The anisotropic displacement parameters were refined for all atoms at all temperature points. The unit-cell parameters were refined using the least-squares techniques. The Olex2 1.5 program package [30] with implemented SHELXL algorithms [31] was used for all structural calculations. All bond lengths and polyhedral volumes in the crystal structures at all temperatures (Table S2) were calculated using rigid-body motion correction in the CrystChemLib program [32], following the formula provided by Downs [33]. The calculation of the thermal-expansion coefficients (TECs) and their visualization was performed using the TTT program package using a linear approximation of the temperature dependencies of the unit-cell parameters [34].

The Raman spectrum of drugmanite (Table S3) was obtained at ambient conditions using a Senterra (Bruker, Billerica, MA, USA) Raman spectrometer conjugated with an Olympus BX-51 microscope using a 785 nm solid state laser as excitation source. The laser power under the 20x objective with a numerical aperture of 0.4 was about 10 mW. The Raman spectrum from the unoriented sample was obtained in the range of 70–1500  $\text{cm}^{-1}$  with a spectral resolution of about 0.9  $\text{cm}^{-1}$ . The accumulation time was 150 s with 2 repetitions. In the obtained spectrum, the piecewise linear baseline was subtracted, and the [0, 1] intensity normalization procedure was performed for clarity.

### 3 Results

#### 3.1 Chemical composition and Raman spectroscopy

The obtained EDS compositional data for the studied drugmanite sample is given in Table 1. Contents of other elements with atomic numbers higher than that of carbon are below detection limits. The empirical formula of drugmanite is  $\text{Pb}_{1.98}(\text{Fe}_{0.87}\text{Al}_{0.12}\text{Sb}^{5+}_{0.01})_{\Sigma 1.01}\text{P}_{2.00}\text{O}_7(\text{OH})_{3.00}$ . Fe was considered as trivalent following van Tassel et al. [35], who assumed that the oxidized environment and the similarity to other arsenate and phosphate mineral assemblages surrounding drugmanite are not likely to contain divalent iron. Additionally, bond valence sums (BVS) [36] were calculated (Table S4), which supports that the *M* site is occupied by trivalent cations only, while the *A* site (Pb) is divalent.

The Raman spectrum of drugmanite was obtained for the first time in the range of 70–1500  $\text{cm}^{-1}$  (Fig. 1). Attempts to acquire the Raman spectrum in the 1500–4000  $\text{cm}^{-1}$  region using all available lasers (488, 514 and 785 nm) were unsuccessful, as the Raman

**Table 1** Chemical composition of drugmanite from Richelle

Constituent	Wt.%	Range	Stand. Dev.	Wt.%
PbO	64.40	62.37–69.91	3.16	64.37
Fe <sub>2</sub> O <sub>3</sub>	10.13	8.60–10.97	0.94	8.85
Al <sub>2</sub> O <sub>3</sub>	0.97	0.68–1.49	0.32	1.61
Sb <sub>2</sub> O <sub>5</sub>	0.14	0.00–0.39	0.18	-
P <sub>2</sub> O <sub>5</sub>	20.68	20.44–20.99	0.24	20.37
H <sub>2</sub> O*	3.94			3.87
<b>Total</b>	<b>100.26</b>			<b>99.07</b>
Reference	This study			[35]

\*Calculated by stoichiometry; - below detection limits

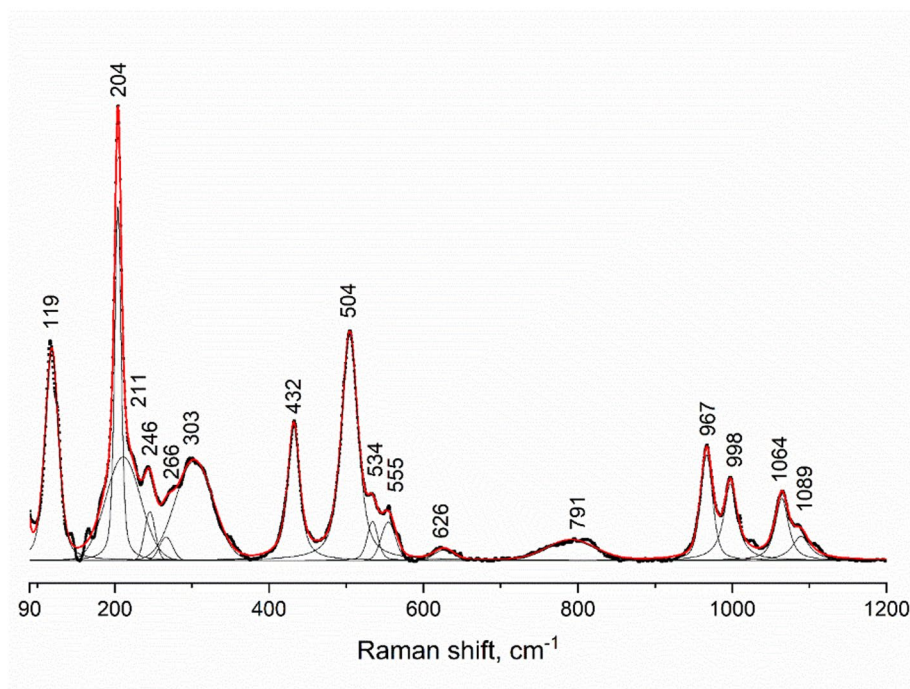


**Fig. 1** Raman spectrum of drugmanite. The experimental spectrum is shown in black (thick) and can be modelled (red) as a superposition of the peaks (thin black)

signal was strongly overwhelmed by the luminescence. It can be interpreted similarly to hydroxylherderite (Table S3). Thus, bands at 967 and 998  $\text{cm}^{-1}$  can be attributed to  $\text{HOPO}_3$  units and the symmetric stretching mode of the  $\text{PO}_4$  units, respectively. The bands in the range of 400–650  $\text{cm}^{-1}$  correspond to the bending modes of the  $\text{PO}_4$  and  $\text{H}_3\text{PO}_4$  units. The bands at 266 and 303  $\text{cm}^{-1}$  are connected with stretching vibrations of Fe–O and Pb–O, whereas the bands at 119, 204 and 246  $\text{cm}^{-1}$  are connected with lattice vibrations [19, 37].

It is notable that the most intense peaks are those associated with lattice vibrations: this may be a result of the reduced rigidity of the structure due to the vacancy at the Q site. The same vacancy leads to a decrease in the amount and intensity of bands in the region of 600–900  $\text{cm}^{-1}$ . Drugmanite, in comparison with hydroxylherderite and bergslagite, has a duplet at 1064 and 1089  $\text{cm}^{-1}$ , which can be associated with POH and PO vibrations [18, 37], respectively.

### 3.2 Crystal structure of drugmanite under ambient conditions

Under ambient conditions, the unit cell parameters (Table 2) and crystal structure refinements of drugmanite are in good agreement with previously published data [26]. Its crystal structure can be described as alternating dense layers of  $\text{FeO}_6$  octahedra and  $\text{PbO}_{10}$  polyhedra with ‘pseudo-layers’, consisting of separate  $\text{PO}_4$  tetrahedra (Fig. 2).

Our data indicates that the T site is fully occupied by P ( $\langle\text{P-O}\rangle = 1.533(15)$  Å,  $^{[\text{IV}]}\text{P-O}$  is 1.55 Å [38]; Table S2), and the Q site is vacant. The A-site is fully occupied with Pb ( $\langle\text{Pb-O}\rangle = 2.894(14)$  Å; see Table S2), which is coordinated by 10 oxygens. Such a type of coordination number is not typical for the A site in GSM and related synthetic compounds, but can be realized, if this site is occupied by Pb or Lu [17]. The octahedrally coordinated M-site is shared between Fe and Al with the ratio 0.87:0.13 ( $\langle\text{M-O}\rangle =$

**Table 2** Crystallographic data for drugmanite at 27 °C

Ref.	This work	[26]*
Sp.gr.	$P2_1/c$	
$a$ [Å]	4.645(1)	4.643(3)
$b$ [Å]	7.987(1)	7.986(5)
$c$ [Å]	11.103(1)	11.111(5)
$\beta$ [°]	90.54(1)	90.16(1)
$V$ [Å <sup>3</sup> ]	412.31(4)	411.97

\*– unit cell parameters  $a$  and  $c$  are swapped for comparison

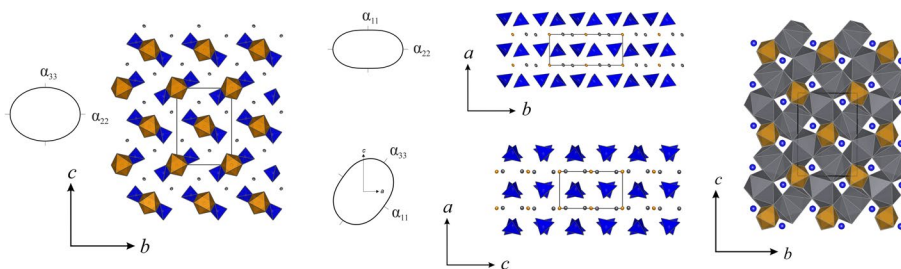


**Fig. 2** Crystal structure of drugmanite in different projections with the section of the thermal-expansion coefficients (TECs) figures in the temperature range of 27 to 400°C. PO<sub>4</sub> tetrahedra and P atoms are given in blue, FeO<sub>6</sub> octahedra and Fe atoms in brown, PbO<sub>10</sub> polyhedra and Pb atoms in grey

2.001(14) Å, while <sup>[VI]</sup>Fe–O and <sup>[VI]</sup>Al–O are 2.045 and 1.935 Å, respectively [38]; see Table S2). The  $\phi$ -site is assumed to be occupied by OH, which is in good agreement with EMPA data.

### 3.3 High-temperature behavior of drugmanite

HT SCXRD experiments showed that drugmanite is stable in the temperature range from 27 to 400 °C. Drugmanite amorphizes between 400 and 500 °C, which is evident by the disappearance of the X-ray diffraction signal for the crystal studied. For the purposes of this study the changes in the unit-cell parameters are considered approximately linear (Fig. 3), as the crystal structure of the mineral undergoes a continuous expansion. The thermal expansion is less anisotropic in comparison to other GSMs (Table 3). The maximal thermal expansion occurs within the pseudo-layer plane ( $cb$ ), while along the  $a$  axis it is slightly lower. This is generally typical for layered crystal structures, but is not obvious for minerals with isolated tetrahedra.

The PO<sub>4</sub> tetrahedra remain stable at all temperatures (see Table S2). The thermal expansion of the structure is due to changes in FeO<sub>6</sub> octahedra and PbO<sub>10</sub> polyhedra, which linearly increase in volume from 10.6(3) to 11.2(3) and from 47.6(7) to 48.8(10) Å<sup>3</sup>, respectively (see Table S2). This process is accompanied by elongation of the average  $M$ –O and Pb–O bonds from 2.001(14) to 2.04(3) Å and from 2.894(14) to 2.92(3) Å at maximum temperature, respectively.

## 4 Discussion

### 4.1 Thermal stability of gadolinite-related minerals and synthetic compounds

The studies on high-temperature behavior of GSM, conducted over the past 8 years [18, 19, 21–24, 39], have shown that the thermal stability range is highly dependent on their chemical composition (Table 3; Fig. 4). According to the obtained data, the most stable minerals are gadolinite-(Y) and hingganite-(Y) (up to ~ 900–1000 °C) [21, 24],

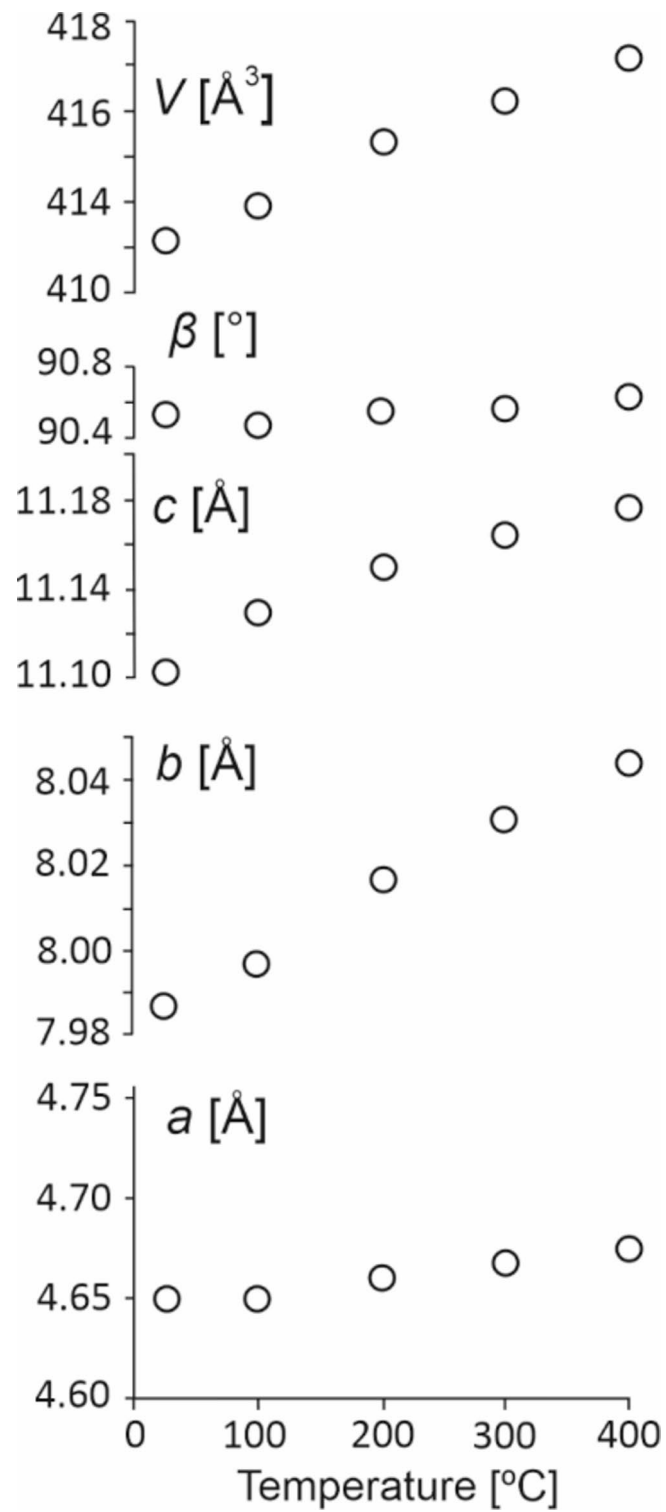


**Fig. 3** Temperature-dependent changes in the unit cell parameters of drugmanite (white circles). The errors are smaller than the symbols

**Table 3** TECs ( $\times 10^6 \text{ }^\circ\text{C}^{-1}$ ) of the gadolinite supergroup minerals and isostructural synthetic compounds along the principal axes ( $\alpha_{ij}$ ) of the thermal expansion tensor, along crystallographic axes at the different temperatures and the ratios of the maximum and minimum thermal expansion axes

A	M	Q	T	$\varphi$	Name	T [°C]	$\alpha_{11}$	$\alpha_{22}$	$\alpha_{33}$	$\mu(\alpha_{33}/\alpha_c)$	$\alpha_a$	$\alpha_b$	$\alpha_c$	$\alpha_\beta$	$\alpha_\gamma$	$\alpha_{\max}/\alpha_{\min}$	Ref.	
Minerals																		
Drugmanite subgroup																		
Pb	Fe <sup>3+</sup>	vacant	P	(OH) <sub>2</sub>	Drugmanite	30–400	13	20	19	45	15	20	17	3	51	1.5	This work	
Herderite subgroup																		
Ca	vacant	Be	P	(OH) <sub>2</sub>	Hydroxylherderite	27–690	15	14	6	21	14	14	7	–4	35	2.6	[19]	
Ca	vacant	Be	As	(OH) <sub>2</sub>	Bergslagitite	(–173)–(+700)	13	14	5	26	12	14	7	4	32	2.9	[18]	
Gadolinite subgroup																		
REE	vacant	Be	Si	(OH) <sub>2</sub>	Hingganite-(Y)	27–900	7	10	3	32	6	10	4	2	20	3.4	[24]	
REE	Fe <sup>2+</sup>	Be	Si	O <sub>2</sub>	Gadolinite-(Y)	30–1050	9	11	7	37	9	11	8	–1	28	1.5	[21]	
Datolite subgroup																		
Ca	vacant	B	Si	(OH) <sub>2</sub>	Datolite	30–710	13	12	4	25	11	12	6	–4	29	3.2	[23]	
Ca	Fe <sup>2+</sup>	B	Si	O <sub>2</sub>	Homilite	30–750	2	16	12	8	2	16	12	–2	30	8	[22]	
Synthetic compounds																		
Tb	Zn	B	B	O <sub>2</sub>	Tb <sub>2</sub> Zn(B <sub>2</sub> O <sub>7</sub> ) <sub>2</sub>	25–800	n/d	n/d	n/d	n/d	~7	~7	~5	n/d	~19	1.4	[39]	

i.e. minerals of the gadolinite subgroup with the beryllium-silicate tetrahedral layers and *REE* in the *A* site. The recent studies of a series of isostructural synthetic compounds demonstrate that *REE* replacement results in sharp increases in the thermal stability range when the size of *REE* cations decreases [40]. As a consequence, one can assume that Yb-dominant species ( $R = 0.985 \text{ \AA}$ ; [38]) will demonstrate a wider range of stability, whereas Nd- and Ce-dominant species ( $R = 1.109$  and  $1.143 \text{ \AA}$ , respectively; [38]) will demonstrate a narrower range of stability. However, as GSMs are not *REE*-specific and contain simultaneously all lanthanides and Y, the only way to check this assumption is to study their synthetic analogues.

Besides, the reason why gadolinite-(Y) is slightly more stable than hingganite-(Y) is the lack of (OH)-groups in gadolinite-(Y). This reason is also appropriate to explain the difference in the thermal stability ranges of datolite and homilite, i.e. borosilicate minerals. Datolite, which has (OH)-groups in the  $\phi$ -site, is stable up to  $710 \text{ }^\circ\text{C}$  [23], whereas its anhydrous analogue, homilite, preserves its initial crystal structure up to  $750 \text{ }^\circ\text{C}$  [22]. It should also be noted that both borosilicate minerals undergo solid-state decomposition with the formation of a melilite-like compound (okayamalite,  $\text{Ca}_2\text{B}_2\text{SiO}_7$ ). An interesting feature of these transformations is that the datolite to okayamalite phase transition resulted in the appearance of a polycrystalline sample instead of a single crystal [23], whereas the homilite to okayamalite phase transition is topotactic, i.e. single-crystal to single-crystal [22]. The thermal stability ranges of bergslagite and hydroxylherderite are very similar (below  $\sim 700 \text{ }^\circ\text{C}$ ) [18, 19], as their chemical composition differs only in that the *T* site is occupied by As and P, respectively, whereas in both cases *M* sites are vacant and  $\phi$ -sites contain (OH)-groups.

Among all studied GSM, drugmanite is the least stable (below  $500 \text{ }^\circ\text{C}$ ). This is most probably associated with two facts as well: (1) vacancy in *Q* site, due to the fact that its crystal structure is not actually layered (see above); and (2) higher content of (OH)-groups, which occupy not only the  $\phi$ -site, but also partially occupy *O* site.

To summarize what has been described in this section, we can say that three aspects determine the stability of GSM under temperature changes:

- (1) The most important aspect is the composition of the tetrahedral layers, i.e. occupancy of *Q* and *T* sites: the most stable minerals are beryllium-containing minerals. A similar tendency has been previously noted for feldspar-related compounds with paracelsian topology [41]. The least stable is the phosphate mineral drugmanite, which has vacancies in tetrahedral layers.
- (2) Among the minerals with similar compositions of tetrahedral layers, more stable are the minerals with dense layers of large cations, i.e. when both *A* and *M* sites are occupied by different cations. If the *M* site is vacant, the mineral is less stable.
- (3) The last important chemical feature affecting GSM stability is the presence of (OH)-groups, which are associated with the vacancy in the *M* site. (OH)-containing minerals are less stable compared with similar anhydrous minerals. Generally, the stability up to about  $700 \text{ }^\circ\text{C}$  is typical for (OH)-containing layered minerals and inorganic compounds [42].

Notably, a number of synthetic gadolinite-related compounds are known:  $\text{Y}_2\text{MnBe}_2\text{Si}_2\text{O}_8\text{O}_2$  [43],  $\text{Yb}_2\text{NiBe}_2\text{Si}_2\text{O}_8\text{O}_2$  [44],  $\text{Gd}_2\text{CdBe}_2\text{Si}_2\text{O}_8\text{O}_2$  [43],  $\beta\text{-ZrB}_2\text{O}_5$  [45],  $\beta\text{-HfB}_2\text{O}_5$  [46],  $\text{Ln}_2\text{Cu}(\text{B}_2\text{O}_5)_2$  ( $\text{Ln} = \text{Tb-Tm, Lu}$ ) [47–50],  $\text{Tb}_2\text{Co}(\text{B}_2\text{O}_5)_2$  [50],  $\text{Ho}_2\text{Ni}(\text{B}_2\text{O}_5)_2$  [51],

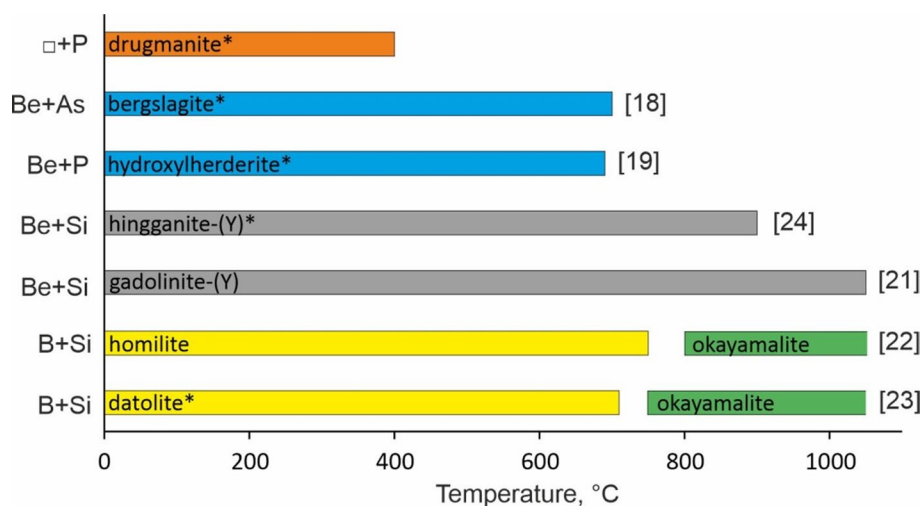


**Fig. 4** Thermal stability ranges of gadolinite supergroup minerals. The "\*" shows the minerals, containing (OH)-groups. The numbers in square brackets show the references

$Ln_2Zn(B_2O_5)_2$  ( $Ln = Eu, Tb, Yb, Lu$ ) [39]. As far as we know, only one of them, namely  $Tb_2Zn(B_2O_5)_2$ , has been studied under high-temperature conditions [39]. This study demonstrated that  $Tb_2Zn(B_2O_5)_2$  is stable up to 800 °C, when it starts to decompose with the formation of  $\mu$ - $TbBO_3$ . Nevertheless, based on the synthesis conditions, we can assume that most synthetic borates with gadolinite-related crystal structures are stable at least up to 1050 °C, as they have been obtained at this or higher temperature [47–49, 51]. As for beryllium silicate compounds [43, 44], which are close to gadolinite based on their chemical composition, they also have to be stable up to about 900–1000 °C by analogy with gadolinite-(Y) and hingganite-(Y).

#### 4.2 Thermal expansion of gadolinite-related minerals and synthetic compounds

At first glance, thermal expansion of GSM varies greatly (Table 3). The volume TECs are in the range of 20 to  $51 \times 10^{-6} \text{ °C}^{-1}$  with the average value, calculated based on all seven studied minerals,  $\langle \alpha_V \rangle_7 = 32 \times 10^{-6} \text{ °C}^{-1}$ . Drugmanite, the crystal structure of which is significantly different, demonstrates the maximum volume expansion ( $\alpha_V = 51 \times 10^{-6} \text{ °C}^{-1}$ ).

It is widely accepted that the main contribution to the TECs values is made by large cations, whereas small tetrahedrally coordinated cations are usually considered as rigid groups [52, 53]. In the case of GSM, these large cations are located at *A* and *M* sites. Such a big difference in the volume TECs of gadolinite supergroup minerals is most probably explained by wide variations in the chemical composition of the *A* and *M* sites. The occupancy of *A* and *M* sites can not be estimated unambiguously, as both of them are always occupied by a complex mixture of different cations. The *A* site is mostly occupied by Ca, Y and Ce, but can contain different cations with charge from 2<sup>+</sup> to 3<sup>+</sup> [17]. The variations of composition in the *M* site are significant too: it is most often occupied by Fe<sup>2+</sup>, but can also include other divalent cations with ionic radius close to Fe<sup>2+</sup> or be vacant or occupied by Fe<sup>3+</sup> [17].

The anisotropy of thermal expansion also varies widely (Table 3). Homilite demonstrates the maximal  $\alpha_{\max}/\alpha_{\min} = 8$  ratio. The reason for such a sharp anisotropy is most probably the oxidation of Fe<sup>2+</sup> to Fe<sup>3+</sup> upon heating, which leads to the decrease in the

unit cell parameters in the temperature range 250–500 °C [22]. This behavior was not observed for any other iron-containing GSM (gadolinite-(Y) and drugmanite). These two minerals, in contrast to homilite, demonstrate the least anisotropy of thermal expansion ( $\alpha_{\max}/\alpha_{\min} = 1.5$ ). In the case of drugmanite, the *M* site is occupied by  $\text{Fe}^{3+}$  initially, i.e. it can not be oxidized. The *M*-site in gadolinite-(Y) is initially occupied by  $\text{Fe}^{2+}$ , but preheating of the sample to 1000 °C in air (for recrystallization) led to iron oxidation [21]. The anisotropy of thermal expansion of minerals with predominantly vacant *M* site (datolite, hingganite-(Y), bergslagite and hydroxylherderite) is in a range from 2.6 to 3.4 (Table 3) and can be associated with different chemical compositions of the *A* site in these minerals. The synthetic  $\text{Tb}_2\text{Zn}(\text{B}_2\text{O}_5)_2$  generally follows the regularities described above: it demonstrates low degrees of anisotropy, as both *A* and *M* sites are fully occupied by cations.

Another interesting aspect of the thermal expansion of GSM is that the direction of maximal thermal expansion is within the layer plane (*cb*), which is not very typical for layered crystal structures. There are two probable reasons for this behavior. First is the existence of quite dense layers of *A* and *M* cations, which fixed the crystal structure and do not allow it to expand perpendicular to the layer plane. Second is the sharp anisotropy of the layer deformation, which can be explained by the flexibility of the four- and eight-membered rings of  $\text{TO}_4$  tetrahedra. The similar behavior has been previously noted for feldspar-related minerals with paracelsian topology [41, 54].

To summarize, we can say that thermal expansion of GSM is a multifaceted process which can not be easily unified and predicted. Nevertheless, it is in agreement with the traditional ideas, according to which the character of thermal deformations of isostructural compounds is determined first of all by the crystal structure and its symmetry, whereas the values of thermal expansion coefficients are determined by the chemical composition and crystal structure [55].

#### 4.3 High-pressure evolution of gadolinite-related minerals and synthetic compounds

The high-pressure behavior has been studied only for 3 GSM (datolite [25], hingganite-(Y) [20] and hydroxylherderite [19]), but, since all of them belong to different subgroups, it allows us to make some generalizations. Additionally, two synthetic gadolinite-related compounds, namely  $\text{ZrB}_2\text{O}_5$  and  $\text{HfB}_2\text{O}_5$ , have been studied upon compression [56]. Generally, all of them demonstrate stability in a wide pressure range.

Datolite ( $Q = \text{B}$ ,  $T = \text{Si}$ ) demonstrates stability in the narrowest range: it undergoes a first-order isosymmetric displacive phase transformation at pressure between 27 and 33 GPa, which is accompanied by the formation of  $\text{Si}_2\text{O}_8$  dimers, consisting of edge-sharing  $\text{SiO}_5$  trigonal bipyramids [25]. This high-pressure modification is stable up to 43 GPa, when it starts to amorphize. The mechanism of this transformation can be described as follows: the eight-membered ring of  $\text{QO}_4$  and  $\text{TO}_4$  tetrahedra elongates along its long diagonal in such a way that along the short diagonal of this ring, the additional fifth oxygen atom enters the coordination sphere of silicon (Fig. 5).

Hingganite-(Y) ( $Q = \text{Be}$ ,  $T = \text{Si}$ ) is stable in the whole studied pressure range (up to 47 GPa) [20]. Generally, the compression mechanism is similar to that described for datolite (Fig. 5). However, due to the difference in chemical composition, the applied pressure is not enough to cause a similar phase transition to occur. It is assumed that hingganite-(Y)

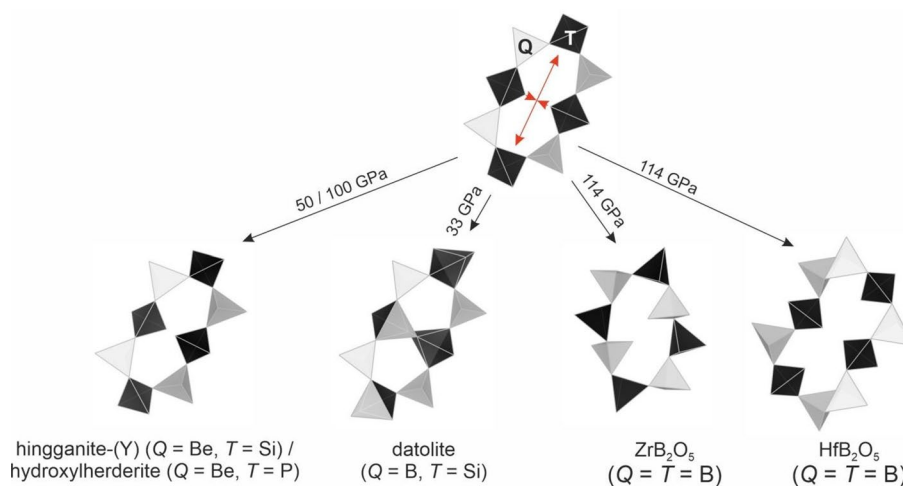


**Fig. 5** The transformation pathways of eight-membered rings upon compression, depending on chemical composition [19, 20, 25, 56]

can undergo a transformation similar to datolite at higher pressure, but there is no confirmation of this to date.

Hydroxylherderite (Q = Be, T = P) is even more stable and preserves its initial crystal structure up to  $\sim 100$  GPa [19]. The quality of the crystal structural data deteriorates significantly above 70 GPa; nevertheless, no phase transition was observed.

The interesting fact is that datolite and hydroxylherderite undergo the maximal compression along the  $a$  axis, i.e. perpendicular to the layer plane, whereas the maximal compression of hingganite-(Y) is within the layer plane. One might assume that by analogy with temperature-induced transformations, the main reason for such differences is the different density of the large cation layer, formed by  $AO_8$  and  $MO_6$  polyhedra or the presence / existence of (OH)-groups. But all three minerals contain (OH)-groups, whereas their  $M$  site is predominantly vacant. Most probably, the difference in compressibility is due to the different size and charge of atoms occupying the  $A$  site. In datolite and hydroxylherderite, the  $A$  site is occupied by  $Ca^{2+}$  ( $R = 1.12$  Å; [38]), whereas in hingganite-(Y) – by  $Y^{3+}$  ( $R = 1.019$  Å; [38]).

The high-pressure studies of the synthetic borates  $ZrB_2O_5$  and  $HfB_2O_5$  with gadolinite-like crystal structures reveal that these compounds are even more stable [56]. Both of them preserve their initial crystal structures up to  $\sim 114$  GPa, when they undergo phase transformations (Fig. 5). Despite the similarity of chemical composition of these two compounds, their high-pressure transformations are fundamentally different. In the case of  $ZrB_2O_5$ , the phase transformation is displacive and is accompanied by a rearrangement of the corner-sharing  $BO_4$  tetrahedra, while still maintaining the four- and eight-membered rings. The obtained high-pressure  $\gamma$ - $ZrB_2O_5$  modification contains highly distorted  $BO_4$  tetrahedra.  $HfB_2O_5$  undergoes a reconstructive phase transition, which leads to the formation of ten-membered rings of distorted  $BO_4$  tetrahedra, which are connected to each other through edges and vertices. The described borates are close to datolite, hingganite-(Y) and hydroxylherderite based on their sites occupancies, i.e. all of them have vacancy in the  $M$  site, the Zr and Hf are small ( $R = 0.83$  and  $0.84$  Å; [38], respectively) and are tetravalent. Most probably, it leads to the increased persistence of the initial crystal structure. Despite the large cations' layers being formed by

highly charged atoms, the maximal compression of both borates is along the  $a$  axis, i.e. perpendicular to the layer plane, which is generally typical for layered crystal structures.

To sum up the above, it can be concluded that gadolinite-like crystal structures are quite stable upon compression. The most stable are borates, then beryllium phosphate and silicate, whereas borosilicate is the least stable. The similarity in the behavior of GSM and feldspar-related minerals with paracelsian topology also lies in the fact that both borosilicate minerals (datolite [25] and danburite  $\text{CaB}_2\text{Si}_2\text{O}_8$  [57]) undergo a phase transformation, accompanied by the formation of rare  $\text{SiO}_5$  polyhedra. At the same time, we did not see the same processes for beryllium phosphate minerals: the high-pressure study of hydroxylherderite [19] did not lead to the formation of such rare structural units as  $\text{BeO}_5$ ,  $\text{PO}_5$ ,  $\text{BeO}_6$  and  $\text{PO}_6$  polyhedra, which have been formed upon compression of hurlbutite,  $\text{CaBe}_2\text{P}_2\text{O}_8$  [58]. Predicting the high-pressure behavior of any minerals or synthetic compounds, based only on their initial crystal structure and chemical composition, without density functional theory calculations, is extremely difficult.

## 5 Conclusion

This study of drugmanite finalizes investigations on the temperature stability and thermal behavior of the gadolinite supergroup minerals. Our understanding of GSM stability could be further expanded by conducting additional high-pressure experiments to determine the elastic behavior and stability ranges of drugmanite, similar to those which were done for datolite, hingganite-(Y) and hydroxylherderite [19, 20, 23].

Including this work, the thermal behavior of all 4 main subgroups in the gadolinite supergroup has been studied. The high-pressure behavior has been studied for three of four subgroups. The performed experiments demonstrate that all the studied minerals are very stable under high-pressure conditions, whereas their stability under high-temperature conditions differs significantly. It has been shown that the composition of the layer, consisting of  $\text{QO}_4$  and  $\text{TO}_4$  tetrahedra, has the greatest influence on the compounds' stability. The density and chemical composition of the large cation ( $A$  and  $M$ ) layers also significantly affect mineral stability. It has to be noted that not only the size, but also the charge of the cations is important. The presence of (OH)-groups only influences the thermal but not the pressure stability of GSM.

## Supplementary Information

The online version contains supplementary material available at <https://doi.org/10.1007/s44346-025-00011-6>.

Supplementary Material 1

### Acknowledgements

The authors thank the X-ray Diffraction Centre, Centre for Optical and Laser Materials Research, and Geomodel Resource Centre of Research Park of Saint Petersburg State University for providing instrumental and computational resources.

### Author contributions

Concept: L.G., A.S. and O.V. Experiments: O.V. and D.V. – Raman spectroscopy, N.V., O.V. and A.K. – chemical composition, L.G., I.K. and A.S. – structural refinements, A.K. – providing sample. Writing and editing: all authors.

### Funding

This manuscript was written at the invitation of the journal's editors and is exempt from article processing charges.

### Data availability

Data will be made available on request.

## Declarations

### Ethics and consent to participate

Not applicable.

### Consent to publish

Not applicable.

### Competing interests

The authors declare no competing interests.

Received: 12 July 2025 / Accepted: 3 November 2025

Published online: 26 November 2025

## References

1. Gadolin J. Undersökning Af En Svart Tung Stenart ifrån Ytterby Stenbrott i Roslagen. *Kungl Svenska Vetenskapsak Handl.* 1794;15:137–55.
2. Klaproth MH. Chemische untersuchung des datoliths. *N Allg J Chem* 1806;6:107–10.
3. Haidinger W. Ueber Den Herderit, eine neue mineralspecies. *Ann Phys* 1828;89:502–5.
4. Szabadvary F. Chapter 73 the history of the discovery and separation of the rare earths. In: Two-hundred-year impact of rare earths on science. Amsterdam: Elsevier; 1988. p. 33–80.
5. Demartin F, Pilati T, Diella V, et al. A crystal-chemical investigation of alpine gadolinite. *Can Mineral.* 1993;31:127–36.
6. Černý P. Rare-element granitic Pegmatites. Part I: anatomy and internal evolution of pegmatitic deposits. *GS.* 1991;18:49.
7. Harlow GE, Hawthorne FC. Herderite from Mogok, Myanmar, and comparison with hydroxyl-herderite from Ehrenfriedersdorf. *Ger Am Mineral.* 2008;93:1545–9.
8. Grew ES. Mineralogy, petrology and geochemistry of beryllium: an introduction and list of beryllium minerals. *Rev Mineral Geochem.* 2002;50:1–76.
9. Zaccarini F, Morales-Ruano S, Scacchetti M, et al. Investigation of datolite ( $\text{CaB}[\text{SiO}_4/(\text{OH})]$ ) from basalts in the Northern apennines ophiolites (Italy): genetic implications. *Geochemistry.* 2008;68:265–77.
10. Lyalina LM, Selivanova EA, Savchenko YE, et al. Minerals of the gadolinite-(Y)-hingganite-(Y) series in the alkali granite pegmatites of the Kola Peninsula. *Geol Ore Deposits.* 2014;56:675–84.
11. Goryainov SV, Krylov AS, Vtyurin AN, et al. Raman study of datolite  $\text{CaBSiO}_4(\text{OH})$  at simultaneously high pressure and high temperature. *J Raman Spectrosc.* 2015;46:177–81.
12. Konerskaya LP, Orlova RG, Boganis EP et al. Using datolite and diopside raw materials in the electrical engineering industry. *Glass Ceram.* 1988;45:199–201.
13. Farsiyants S, Opaleichuk LS, Romanova VI. New types of filters. *Glass Ceram.* 1989;46:338–9.
14. Tarasevich BP, Isaeva LB, Kuznetsov EV, et al. Boron building ceramic protecting against neutron radiation. *Glass Ceram.* 1990;47:175–8.
15. Mann KS, Sidhu GS. Verification of some low-Z silicates as gamma-ray shielding materials. *Ann Nucl Energy.* 2012;40:241–52.
16. Malczewski D, Dziurawicz M. 222 Rn and 220 Rn emanations as a function of the absorbed  $\alpha$ -doses from select metamict minerals. *Am Mineral.* 2015;100:1378–85.
17. Bačík P, Miyawaki R, Atencio D, et al. Nomenclature of the gadolinite supergroup. *Eur J Mineral.* 2017;29:1067–82.
18. Shagova AK, Gorelova LA, Vereshchagin OS, et al. Thermal stability, low- and high-temperature behavior of bergslagit, a beryllioarsenate member of the gadolinite supergroup. *Phys Chem Miner.* 2025;52:8. <https://doi.org/10.1007/s00269-025-01311-1>.
19. Gorelova L, Vereshchagin O, Aslandukov A, et al. Hydroxylherderite ( $\text{Ca}_2\text{Be}_2\text{P}_2\text{O}_8(\text{OH})_2$ ) stability under extreme conditions (up to 750°C/100 GPa). *J Am Ceram Soc.* 2023;106:2622–34.
20. Gorelova LA, Pakhomova AS, Krivovichev SV, et al. Compressibility of hingganite-(Y): high-pressure single crystal X-ray diffraction study. *Phys Chem Miner.* 2020;47:22. <https://doi.org/10.1007/s00269-020-01090-x>.
21. Gorelova LA, Panikorovskii TL, Pautov LA, et al. Temperature-versus compositional-induced structural deformations of gadolinite group minerals with various Be/B ratio. *J Solid State Chem.* 2021;299:122187.
22. Gorelova LA, Vereshchagin OS, Shagova AK, et al. Topotactic transformation of gadolinite- to melilite-type structure revisited. *J Am Ceram Soc.* 2024;107:3534–49.
23. Krzhizhanovskaya MG, Gorelova LA, Bubnova RS, et al. High-temperature crystal chemistry of layered calcium borosilicates:  $\text{CaBSiO}_4(\text{OH})$  (datolite),  $\text{Ca}_4\text{B}_5\text{Si}_3\text{O}_{15}(\text{OH})_5$  ('bakerite') and  $\text{Ca}_2\text{B}_2\text{SiO}_7$  (synthetic analogue of okayamalite). *Phys Chem Minerals.* 2018;45:463–73.
24. Vereshchagin OS, Gorelova LA, Shagova AK, et al. Re-investigation of 'minasgeraisite-(Y)' from the Jaguaraçu pegmatite, Brazil and high-temperature crystal chemistry of gadolinite-supergroup minerals. *MinMag.* 2023;87:470–9.
25. Gorelova LA, Pakhomova AS, Aprilis G, et al. Pentacoordinated silicon in the high-pressure modification of datolite,  $\text{CaBSiO}_4(\text{OH})$ . *Inorg Chem Front.* 2018;5:1653–60.
26. King GSD, Sengier-Roberts L, Drugmanite.  $\text{Pb}_2(\text{Fe}_{0.78}\text{Al}_{0.22})\text{H}(\text{PO}_4)_2(\text{OH})_2$ : its crystal structure and place in the datolite group. *Bull Minér.* 1988;111:431–7.
27. Korniyakov IV, Samarkina NK, Izatulina AR, et al. High-temperature powder versus single-crystal X-ray diffraction studies: which method to choose? Thermal behavior of shumwayite,  $[(\text{UO}_2)(\text{SO}_4)(\text{H}_2\text{O})_2]_2 \cdot \text{H}_2\text{O}$ . *J Appl Crystallogr.* 2025;58:1615–26.
28. Gorelova L, Vereshchagin O, Kasatkin A. Thermal expansion and polymorphism of slawsonite  $\text{SrAl}_2\text{Si}_2\text{O}_8$ . *Minerals.* 2021;11:1150.
29. Agilent Technologies. *CrysAlisPRO*. Oxford: Oxford Diffraction; 2012.
30. Dolomanov OV, Bourhis LJ, Gildea RJ, et al. OLEX2: a complete structure solution, refinement and analysis program. *J Appl Crystallogr.* 2009;42:339–41.
31. Sheldrick GM. A short history of SHELX. *Acta Crystallogr A.* 2008;64:112–22.

32. Rashchenko SV. Crystchemlib: a python library and GUI for analysis of crystal structure datasets. *J Appl Crystallogr.* 2025;58:290–5.
33. Downs RT. Analysis of harmonic displacement factors. *Rev Miner Geochem.* 2000;41:61–87.
34. Bubnova RS, Firsova VA, Filatov SK. Software for determining the thermal expansion tensor and the graphic representation of its characteristic surface (theta to tensor-TTT). *Glass Phys Chem (Glass Phys Chemistry).* 2013;39:347–50.
35. van Tassel R, Fransolet AM, Abraham K. Drugmanite  $Pb_2(Fe^{3+}, Al)(PO_4)_2(OH) \cdot H_2O$ , a new mineral from Richelle. *Belgium Min Mag.* 1979;43:463–7.
36. Brese NE, O'Keeffe M. Bond-valence parameters for solids. *Acta Crystallogr B Struct Sci.* 1991;47:192–7.
37. Frost RL, Scholz R, López A, et al. Raman, infrared and near-infrared spectroscopic characterization of the herderite-hydroxylherderite mineral series. *Spectrochim Acta Mol Biomol Spectrosc.* 2014;118:430–7.
38. Shannon RD. Revised effective ionic radii and systematic studies of interatomic distances in halides and chalcogenides. *Acta Cryst A.* 1976;32:751–67.
39. Teichtmeister TA, Förster T, Bernhart AH, et al. High-Pressure/High-Temperature synthesis of the lanthanoid zinc Borates  $Ln_2Zn(B_2O_3)_2$  ( $Ln = Eu, Tb, Yb, Lu$ ) with a Gadolinite-Analogue crystal structure and luminescence properties of  $Tb_2Zn(B_2O_3)_2 \cdot Eu^{3+}$ . *Chem Mater.* 2024;36:11462–77.
40. Krzhizhanovskaya MG, Vereshchagin OS, Kopylova Y, et al. The structural origin and boundaries of thermal transitions in stillwellite-type  $LnBSiO_5$ . *Opt. Mater.* 2024;147:114651.
41. Gorelova LA. Phase transformations in feldspar group minerals with paracelsian topology under high temperature and high pressure. *Russ Geol Geophys.* 2023;64:950–61.
42. Földvári M. Handbook of thermogravimetric system of minerals and its use in geological practice. Occasional papers of the Geological Institute of Hungary. Volume 213. Budapest: Geological Inst. of Hungary; 2011.
43. Ito J. The synthesis of gadolinite. *Proc Jpn Acad.* 1965;41:404–7.
44. Foit FF, Gibbs GV. Refinement of  $NiYb_2Be_2Si_3O_{10}$ , a gadolinite-type structure. *Z Kristallogr - Cryst Mater.* 1975;141:375–86.
45. Knyrim JS, Huppertz H. High-pressure synthesis, crystal Structure, and properties of the first ternary zirconium Borate  $\beta$ - $ZrB_2O_5$ . *Z Naturforsch B.* 2008;63:707–12.
46. Knyrim JS, Huppertz H. High-pressure synthesis, crystal structure, and properties of the first ternary hafniumborate  $\beta$ - $HfB_2O_5$ . *J Solid State Chem.* 2007;180:742–8.
47. Schaefer J, Bluhm K. Synthese und Kristallstruktur von  $CuLn_2[B_2O_3]_2$  ( $Ln = Er^{3+}, Lu^{3+}$ ): Zwei kupferlanthanoidborate Mit  $2\infty [B_2O_3]^{4-}$ -Anionen / Synthesis and crystal structure of  $CuLn_2[B_2O_3]_2$  ( $Ln = Er^{3+}, Lu^{3+}$ ): two copper lanthanoid Borates with  $2\infty [B_2O_3]^{4-}$ -Anions. *Z Naturforsch B.* 1995;50:1141–5.
48. Schaefer J, Bluhm K.  $CuTm_2[B_2O_3]_2$ : Das erste „Metaborat Mit einem  $2\infty [B_2O_3]^{4-}$ -Anion /  $CuTm_2[B_2O_3]_2$ : the first metaborate with a  $2\infty [B_2O_3]^{4-}$ -Anion. *Z Naturforsch B.* 1995;50:630–4.
49. Wiesch A, Bluhm K.  $CuHo_2[B_2O_3]_2$ : Ein unerwarteter Strukturtyp in der reihe der Kupferlanthanoidborate /  $CuHo_2[B_2O_3]_2$ : an unexpected structure type in the series of copper lanthanoid Borates. *Z Naturforsch B.* 1998;53:5–8.
50. Teichtmeister TA, Hladik MM, Heymann G, et al.  $Tb_2Co(B_2O_3)_2$  and  $Tb_2Cu(B_2O_3)_2$  – two new Borates with gadolinite-type structures. *Z Naturforsch B.* 2023;78:381–8.
51. Bluhm K, Wiesch A. Synthese und Kristallstruktur von  $NiHo_2(B_2O_3)_2$ , Das erste nickellanthanoidborat Mit einem  $2\infty [B_2O_3]^{4-}$ -Anion / Synthesis and crystal structure of  $NiHo_2(B_2O_3)_2$ , the first nickel lanthanoid Borate with a  $[B_2O_3]^{4-}$ - anion. *Z Naturforsch B.* 1996;51:677–80.
52. Dove MT, Pryde AKA, Keen DA. Phase transitions in tridymite studied using 'Rigid unit mode' theory, reverse Monte Carlo methods and molecular dynamics simulations. *MinMag.* 2000;64:267–83.
53. Dove M, Palmer, Cool, et al. On the role of Al-Si ordering in the cubic-tetragonal phase transition of leucite. *Am Miner.* 1993;78:486–92.
54. Gorelova LA, Filatov SK, Krzhizhanovskaya MG, et al. High temperature behaviour of danburite-like borosilicates  $MB_2Si_2O_8$  ( $M = Ca, Sr, Ba$ ). *Phys Chem Glasses: Eur J Glass Sci Technol B.* 2015;56:189–96.
55. Filatov SK. High-temperature crystal chemistry. Leningrad: Nedra; 1990.
56. Pakhomova A, Fuchs B, Dubrovinsky LS, et al. Polymorphs of the Gadolinite-Type Borates  $ZrB_2O_5$  and  $HfB_2O_5$  under extreme pressure. *Chem Eur J.* 2021;27:6007–14.
57. Pakhomova A, Bykova E, Bykov M, et al. A closer look into close packing: pentacoordinated silicon in a high-pressure polymorph of danburite. *IUCrJ.* 2017;4:671–7.
58. Pakhomova A, Aprilis G, Bykov M, et al. Penta- and hexa-coordinated beryllium and phosphorus in high-pressure modifications of  $CaBe_2P_2O_8$ . *Nat Commun.* 2019;10:2800.

## Publisher's note

Springer Nature remains neutral with regard to jurisdictional claims in published maps and institutional affiliations.